

Elsevier Editorial System(tm) for Nuclear Inst. and Methods in Physics Research, A
Manuscript Draft

Manuscript Number:

Title: Time-Resolved Data Acquisition for In Situ Subsurface Planetary Geochemistry

Article Type: Research Paper

Section/Category: Special Applications

Keywords: Elemental analysis, pulsed neutron generator, time-tagged data acquisition, optimized time-gating, time-dependent neutron and gamma-ray detection

Corresponding Author: Ms. Julia Gates Bodnarik, M.S.

Corresponding Author's Institution: NASA Goddard Space Flight Center

First Author: Julia Gates Bodnarik, M.S.

Order of Authors: Julia Gates Bodnarik, M.S.; Dan M Burger, B.S.; Arnold Burger, Ph.D.; Larry G Evans, Ph.D.; Ann M Parsons, Ph.D.; Jeffrey S Schweitzer, Ph.D.; Richard D Starr, Ph.D.; Keivan G Stassun, Ph.D.

Abstract: The current gamma-ray/neutron instrumentation development effort at NASA Goddard Space Flight Center aims to extend the use of active pulsed neutron interrogation techniques to probe the subsurface geochemistry of planetary bodies in situ. All previous NASA planetary science missions, that used neutron and/or gamma-ray spectroscopy instruments, have relied on a constant neutron source produced from galactic cosmic rays. One of the distinguishing features of this effort is the inclusion of a high intensity 14.1 MeV pulsed neutron generator synchronized with a custom data acquisition system to time each event relative to the pulse. With usually only one opportunity to collect data, it is difficult to set a priori time-gating windows to obtain the best possible results. Acquiring time-tagged, event-by-event data from nuclear induced reactions provides raw data sets containing channel/energy, and event time for each gamma ray or neutron detected. The resulting data set can be plotted as a function of time or energy using optimized analysis windows after the data are acquired. Time windows can now be chosen to produce energy spectra that yield the most statistically significant and accurate elemental composition results that can be derived from the complete data set. The advantages of post-processing gamma-ray time-tagged event-by-event data in experimental tests using our prototype instrument will be demonstrated.

Dear NIM-A Editors:

This cover letter accompanies the submission of the paper: "Time-Resolved Data Acquisition for *In Situ* Subsurface Planetary Geochemistry" for publication in NIM-A.

This paper contains 8 figures and 3 tables. Black and white copies of the figures will be provided for the print version and the enclosed color figures are the web version.

This work has not been published previously in a referred journal and is not under consideration at this time in any other journal.

Possible referees you might wish to consider for this paper are:

- 1) Dr. William V. Boynton; email: wboynton@lpl.arizona.edu
- 2) Dr. Russel Hertzog; email: russelhertzog@gmail.com
- 3) Dr. David Chichester; email: david.chichester@inl.gov

I hope these instructions and the accompanying manuscript and figures are clearly organized and understandable. Please do not hesitate to contact me with questions.

Sincerely,

Julia G. Bodnarik, Corresponding Author
NASA/Goddard Space Flight Center
Solar System Exploration Division
Astrochemistry Laboratory
Code 691
Greenbelt, Maryland 20771

Phone: (301) 286-1398
Mobile: (808) 896-6759
FAX: (301) 286-1683
email: julia.g.bodnarik@nasa.gov; julie.g.bodnarik@gmail.com

1 **Time-Resolved Data Acquisition for *In Situ* Subsurface Planetary**

2 **Geochemistry**

3

4 Author List:

5 J. G. Bodnarik^{a,b*}, D. M. Burger^c, A. Burger^d, L. G. Evans^e, A. M. Parsons^a, J. S.

6 Schweitzer^f, R. D. Starr^g, K. G. Stassun^b

7

8 ^aNASA Goddard Space Flight Center, 8800 Greenbelt Rd., Code 691, Greenbelt,

9 MD 20771, USA; e-mail: julia.g.bodnarik@nasa.gov, ann.m.parsons@nasa.gov,

10 ^bVanderbilt University, Department of Physics and Astronomy, VU Station B

11 #1807, Nashville, TN 37235, USA; e-mail: keivan.stassun@vanderbilt.edu

12 ^cVanderbilt University, VU Station B #351679, 2301 Vanderbilt Place, Nashville,

13 TN 37235-1679, USA; e-mail: dan.burger@vanderbilt.edu

14 ^dFisk University, Department of Physics, 240 W.E.B. DuBois Hall, 1000 17th Ave.

15 N., Nashville, TN, 37208, USA; e-mail: aburger@fisk.edu

16 ^eComputer Sciences Corporation, 7900 Harkins Rd., Lanham, MD 20706, USA;

17 email: larry.g.evans@nasa.gov

18 ^fUniversity of Connecticut, Department of Physics, Storrs, CT 06269-3046, USA;

19 email: schweitz@phys.uconn.edu

20 ^gCatholic University of America, Institute for Astrophysics and Computational

21 Sciences, Washington, D.C., 20064, USA; email: richard.d.starr@nasa.gov

22

* Corresponding author. Tel.: provided in cover letter; fax: provided in cover letter;
e-mail: julia.g.bodnarik@nasa.gov

23 **Abstract:**

24 The current gamma-ray/neutron instrumentation development effort at NASA
25 Goddard Space Flight Center aims to extend the use of active pulsed neutron
26 interrogation techniques to probe the subsurface geochemistry of planetary
27 bodies *in situ*. All previous NASA planetary science missions, that used neutron
28 and/or gamma-ray spectroscopy instruments, have relied on a constant neutron
29 source produced from galactic cosmic rays. One of the distinguishing features of
30 this effort is the inclusion of a high intensity 14.1 MeV pulsed neutron generator
31 synchronized with a custom data acquisition system to time each event relative
32 to the pulse. With usually only one opportunity to collect data, it is difficult to set
33 *a priori* time-gating windows to obtain the best possible results. Acquiring time-
34 tagged, event-by-event data from nuclear induced reactions provides raw data
35 sets containing channel/energy, and event time for each gamma ray or neutron
36 detected. The resulting data set can be plotted as a function of time or energy
37 using optimized analysis windows after the data are acquired. Time windows
38 can now be chosen to produce energy spectra that yield the most statistically
39 significant and accurate elemental composition results that can be derived from
40 the complete data set. The advantages of post-processing gamma-ray time-
41 tagged event-by-event data in experimental tests using our prototype instrument
42 will be demonstrated.

43

44 Keywords: Elemental analysis, pulsed neutron generator, time-tagged data
45 acquisition, optimized time-gating, time-dependent neutron and gamma-ray
46 detection

47

48 **1. Introduction**

49 The objective of the current gamma-ray/neutron instrumentation development
50 at NASA Goddard Space Flight Center (GSFC)¹ is to use active pulsed neutron
51 interrogation techniques to determine *in situ* the subsurface bulk elemental
52 concentrations of planetary bodies. To date, all the planetary science missions
53 that have included both neutron and gamma-ray instruments have made remote
54 sensing measurements from orbit or during close fly-by encounters with a
55 planetary body (e.g. Lunar Prospector [1], Mars Odyssey [2,3], Dawn [4],
56 MESSENGER [5], NEAR [6], and LRO [7,8]). The excitation sources for these
57 remote sensing measurements have necessarily been limited to the high energy

¹ Abbreviations:

PNG – Pulsed Neutron Generator

PING – Pulsing In situ with Neutrons and Gamma rays

GSFC – Goddard Space Flight Center

MESSENGER – MErcury Surface, Space ENvironment, GEOchemistry and Ranging

LRO – Lunar Reconnaissance Orbiter

NEAR – Near Earth Asteroid Rendezvous

GRC – Galactic Cosmic Rays

MCNPX – Monte Carlo N-Particle eXtended

DSA – Digital Signal Analyzer

PHA – Pulse Height Analysis

TLIST – Time-stamped LIST

HPGe – High Purity Germanium

GGAO – Goddard's Geophysical and Astronomical Observatory

58 (fast) neutrons that are produced when Galactic Cosmic Rays (GCR) interact
59 with planetary materials. Although GCR-generated fast neutron rates change
60 with the 11-year solar cycle, they occur at a constant rate for these
61 measurements time. Measured gamma-ray spectra contain all of the gamma ray
62 lines from each of the gamma ray-producing interactions of neutrons with the
63 planetary material. Gamma-ray spectra thus include peaks resulting from
64 inelastic scattering, thermal neutron capture, delayed activation and natural
65 radioactivity. However, the large number of peaks and the high spectral
66 background result in peak interferences, misidentifications and reduced precision
67 in the reported gamma-ray results. These difficulties are avoided for *in situ*
68 measurements of a landed instrument package that includes a Pulsed Neutron
69 Generator (PNG) as the excitation source. A PNG can produce fast neutrons at
70 ~100 times greater rate than GCR interactions resulting in significantly reduced
71 measurement times for equivalent sensitivity. A PNG can also produce 14.1
72 MeV neutrons in relatively short bursts with an adjustable neutron pulse period
73 and width. With the production of the high-energy neutrons restricted to the
74 duration of the burst, the gamma rays that result from the inelastic scattering of
75 these fast neutrons will also occur only during the time of the burst. Between
76 each burst, the planetary material moderates the fast neutrons so that the
77 gamma rays are largely produced by thermal neutron capture. After most of the
78 thermal neutrons have been absorbed, the gamma rays resulting from delayed
79 activation and natural radioactivity become visible. Separating the gamma rays
80 by their detection time relative to a PNG pulse results in lower background and a

81 substantial reduction in peak interferences, while capturing essentially all of the
82 gamma rays due to a particular type of reaction. Separating gamma ray spectra
83 by physical process minimizes the systematic effects from interfering peaks and
84 provides improved precision and accuracy in the peak analysis that directly
85 results in more precise elemental concentration measurements. We have
86 previously shown [9] that significant improvements in precision can be obtained
87 using properly chosen time windows for time-gated coincidence data acquisition
88 methods. Here we report the increased benefits of using time tagged event-by-
89 event data.

90 On Earth, it is possible to adjust the PNG pulse period and width as well as the
91 coincident data acquisition window timing parameters for an optimum analysis of
92 a sample because one usually has a general idea of the sample's bulk
93 composition and its properties with regard to neutron and gamma ray transport.
94 Even without this knowledge, multiple measurements using adjusted parameters
95 are usually possible. So it is often simple and sufficient to use coincidence data
96 acquisition methods with a limited number of fixed time gates for these ground-
97 based experiments on Earth. However, one rarely has the luxury of repeating
98 measurements on another planet. When making *in situ* measurements on a
99 planetary body, there is often a great ignorance of its composition especially with
100 regard to elements that affect the neutron and gamma ray time dependence. For
101 planetary science applications it would be very difficult to make multiple
102 measurements at a variety of different timing conditions with sufficient statistics
103 to determine the optimum timing parameters. The optimal timing parameters

104 largely depend on neutron transport properties that are governed by effects that
105 vary by location such as elemental composition, hydrogen content, density and
106 subsurface layering geometries. By the time one has determined what the
107 proper time gating should be, the mission may be over, or, in the case of a rover
108 mission, the rover may have already left the region where the earlier data were
109 obtained.

110 This type of problem has been addressed in early NASA Apollo gamma ray
111 experiments [10] as well as in other scientific fields such as radioanalytical
112 chemistry applications [11] by accumulating data on an event-by-event basis
113 where the energy and measurement time is recorded for every event detected
114 during the data acquisition time. When data are accumulated in an event-by-
115 event mode that includes event times, one can analyze the data after the
116 measurement has been made (post-processing) to determine the optimum time
117 windows for spectral data analysis. Although event-by-event data acquisition
118 leads to large raw data files, it makes it possible to perform the optimal spectral
119 analysis without requiring repeated measurements.

120 *1.1 The Probing In situ with Neutrons and Gamma rays (PING) Instrument*

121 Our group at NASA/GSFC is currently developing the Probing *In situ* with
122 Neutrons and Gamma rays (PING) instrument for planetary *in situ* bulk elemental
123 composition measurements [9] by leveraging both well-established oil well and
124 scientific logging techniques [12] and remote sensing planetary gamma-ray
125 spectroscopy techniques. PING employs a 14.1 MeV pulsed neutron generator
126 to excite materials at and below a planetary surface and utilizes the penetrating

127 nature of these fast neutrons and gamma rays to probe the subsurface soil
128 composition over a 1 m² area and down to depths of 10-100 cm. PING's gamma-
129 ray spectrometer and neutron detectors measure the resulting gamma rays and
130 neutrons that emerge from the planetary surface. To illustrate an example
131 application, PING is shown in Figure 1 attached to the underside of a planetary
132 rover.

133 < Insert Figure 1 >

134 A gamma-ray spectrometer measures the resulting inelastic scattering, capture,
135 and delayed activation gamma rays emitted by the excited elements as well as
136 gamma rays emitted from natural radioactive decay; neutron detectors measure
137 the number of the epithermal and thermal neutrons that reach the surface as a
138 function of time relative to the initiation of each high-energy neutron pulse. PING
139 gamma-ray and neutron data are acquired using custom software to control
140 digital signal analyzer electronics. These data, coupled with MCNPX [13]
141 computer simulations, let us quantitatively determine the bulk elemental
142 composition of the subsurface material for any solid body in the Solar System,
143 even bodies with a dense atmosphere. PING can measure a wide range of
144 elements (e.g. C, H, O, P, S, Si, Na, Ca, Ti, Fe, Al, Cl, Mg, Mn, K, Th, and U)
145 depending on their abundance in the planetary material.

146 *1.2 Outdoor Neutron-Gamma Ray Instrument Test Site*

147 We are testing the capabilities of our PING instrument prototypes at a unique
148 outdoor gamma ray and neutron instrumentation testing facility located at
149 Goddard's Geophysical and Astronomical Observatory (GGAO) near Goddard's

150 main campus. A schematic view of the test site is shown in Figure 2. This test
151 facility allows us to operate PING on top of either of two large, well-characterized
152 granite and basalt monuments, each 1.8 m x 1.8 m x 0.9 m in size. Activation
153 Laboratories Ltd. in Ancaster, Ontario, Canada, has independently measured the
154 full elemental compositions of these Concord Gray Granite and Columbia River
155 Basalt materials to the ppm level. PING is remotely operated from a building
156 more than 75 m from the monuments due to the radiation hazard from the PNG's
157 14 MeV neutrons. Underground power and communications lines connect the
158 operations building to the test monuments. Details of the specific PING
159 measurements are given in Section 3.1 and further information about the test
160 facility can be found in [14,15].

161 < Insert Figure 2 >

162 *1.3 Using TLIST Data to Improve PING Elemental Composition Measurements*

163 A Canberra Lynx Digital Signal Analyzer (DSA) is used to acquire data from
164 each gamma ray and neutron detector used for a PING measurement. While the
165 Lynx DSA hardware [16], features multiple data acquisition modes, including
166 coincidence-gated Pulse Height Analysis (PHA) and event-by-event Time-
167 stamped LIST (TLIST) mode, operation of the Lynx DSAs in TLIST mode
168 required the development of custom software. In this paper, we describe both the
169 acquisition of TLIST data using our custom MultiScan software [17] and the post-
170 processing of our data that allows us to:

- 171 1) Use optimized timing windows to separate the data into distinct gamma-
172 ray spectra resulting from either a) inelastic scattering, during the neutron

173 pulse, b) thermal neutron capture, between neutron pulses, or c) delayed
174 activation and natural activity events visible just before the next fast neutron
175 pulse. This separation allows us to more accurately identify gamma ray lines
176 and more precisely measure gamma ray net peak areas;

177 2) Isolate a particular energy line from a gamma ray spectrum and observe
178 its intensity time profile with respect to the PNG pulse to more accurately
179 identify and measure the gamma-ray line and its net peak area; and

180 3) Extract gamma ray data to optimize the timing windows needed to look
181 for specific elements in different environments and to obtain the optimum
182 precision for the analyzed peak intensities.

183

184 **2. The TLIST Data Acquisition Technique**

185 Analyzing individual gamma-ray peaks in a traditional PHA energy spectrum
186 can be challenging due to both interfering lines and the background continuum
187 resulting from multiple processes. We reduce these effects and obtain higher
188 gamma-ray line sensitivity with increased signal-to-noise by recording gamma-
189 ray time and energy in an event-by-event mode. We use our custom MultiScan
190 software and the Canberra Lynx DSA in TLIST mode to record the energy and
191 time (temporal resolution $0.1 \mu\text{s}$) of each event detected during a PNG pulse
192 cycle. As discussed in Section 1, we obtain a master data set that is not limited
193 to predetermined coincidence timing gates set for specific nuclear processes.
194 This master data set can be sliced in many ways without loss of information or
195 requiring additional measurements with different data acquisition window settings.

196 Figures 3a and b illustrate the results of our post-processing of TLIST gamma-
197 ray data for various timing windows.

198 < Insert Figures 3a and 3b>

199 Figure 3a is an illustration of the PNG fast neutron pulse train and the intra-
200 pulse location of the different timing windows needed to separate the gamma
201 rays that result from the inelastic scattering, thermal neutron capture, delayed
202 activation and natural radioactivity processes. Figure 3b is an illustration of the
203 differences in the resulting energy and intensity of the gamma ray lines and
204 background for each of these separated spectra.

205 *2.1 Custom MultiScan Data Acquisition Software*

206 Lynx DSA data acquisition can be performed using either the Lynx web-based
207 interface or the Genie 2000 software package [16] both available from Canberra
208 Industries. Although the Lynx DSA hardware offers the required TLIST mode,
209 neither of these software options provides the flexibility and all of the capabilities
210 we need for our specific instrument application. The MultiScan software,
211 designed specifically for our project, allows us to 1) acquire data in TLIST mode
212 while synchronized to the PNG pulse, 2) save data in ASCII format, 3) analyze
213 TLIST data for an unlimited number of time windows, and 4) perform multiple
214 consecutive data acquisitions while maintaining the Lynx graphical analysis and
215 configuration features. Example images of the MultiScan software interface are
216 shown in Figure 4.

217 < Insert Figure 4>

218 The MultiScan software was written in Java, since we needed to make the
219 code cross-platform and easy to understand so that others can make changes to
220 the code when necessary. When starting a new data acquisition or scan, the user
221 can specify which of the multiple Lynx DSAs to perform the scan, the acquisition
222 mode (PHA or TLIST), the file format to save the data (Canberra CNF file, ASCII
223 text, or both), how many consecutive scans to perform, and the duration of each
224 scan (in either live time or true time). Settings can be modified quickly and easily
225 within the software. The data are both written to a file and presented in a large
226 display window with multiple data visualization features. The program also
227 provides basic data analysis tools for both PHA and TLIST scans, and off-line
228 TLIST data post-processing time-slicing tools, as well as a diagnostic feature for
229 monitoring the operating parameters within the Lynx DSA [18].

230 *2.2 TLIST Data Analysis Techniques*

231 We use the MultiScan software with Lynx DSAs to acquire TLIST data for
232 gamma-ray and neutron detectors with the start of a data acquisition
233 synchronized with the start of a PNG pulse. Synchronization of the PNG and
234 DSA clocks insures the accuracy of these event times over multi-hour data
235 acquisition runs. Our basic post-processing procedure for the individual event-by-
236 event data files is to take the modulus of the absolute times for the detected
237 events with respect to the known PNG pulse period to derive the time of each
238 event relative to the neutron pulse. The next step is to put all of the files for a
239 given experiment on the same time base. The result is a master data set of
240 energies and relative event times that can be “sliced” in any number of ways.

241 Slicing the data in time means establishing the boundary between times where
242 different nuclear processes dominate. The result is separate gamma-ray spectra
243 for the specific processes that have the event statistics characteristic of the total
244 acquisition time. Slicing the data in energy means establishing energy
245 boundaries around spectral features whose time profile one wishes to study.
246 After generating this master data set with energy and relative time values, we
247 can analyze our gamma ray and neutron data to infer the bulk elemental
248 composition, density, and subsurface layering of planetary bodies.

249 **3. Experiments and Results with TLIST Data**

250 Gamma-ray and neutron spectroscopy is used to infer the bulk elemental
251 concentrations of the surface and subsurface of planetary bodies. The time
252 dependence relative to the neutron burst of gamma ray peaks in an energy
253 calibrated spectrum can be analyzed to determine the neutron-nuclei
254 interaction(s) associated with a particular gamma ray energy. We performed
255 PING experiments using a pulsed neutron generator, gamma ray and neutron
256 detectors on a meter-sized basalt monument. The TLIST data acquired and
257 analyzed in this section only represents 6.33 hours of data acquisition with a
258 fixed neutron pulse with a width of 100 μs and a pulse period of 1000 μs . The
259 results of TLIST data acquisition and post-processing presented will demonstrate
260 the improved precision and reduced systematic errors that can be achieved as
261 compared with pre-assigned acquisition windows from a presumed knowledge of
262 elemental composition.

263 *3.1 Experiment Description*

264 During these experiments, we acquired 6.33-hrs of TLIST data using a Lynx
265 DSA connected to an n-type Ortec GMX Series HPGe portable coaxial detector
266 system and a 14 MeV Deuterium - Tritium Thermo Fisher MP320 portable PNG
267 [19] positioned on top of our Columbia River basalt monument, as shown in
268 Figure 5.

269 < Insert Figure 5 >

270 The Lynx DSA reading out the HPGe detector was connected directly to the
271 PNG to synchronize the start of each data acquisition run with the start of a
272 neutron pulse. The PNG beam current, high voltage, frequency, and duty factor
273 were set to 60 μ A, 50 kV, 1 kHz, and 10% respectively. At these settings, the
274 PNG produced a neutron pulse width, pulse period, energy, and rate of 100 μ s,
275 1000 μ s, 14 MeV, and 3×10^7 n/s respectively.

276 *3.2 Gamma-Ray Peak Separation Using TLIST Data Analysis*

277 Gamma-ray line identification can be difficult for many reasons including: 1)
278 interfering gamma-ray lines resulting from the use of low energy resolution
279 gamma-ray spectrometers (i.e. NaI gamma ray scintillation detectors); and 2)
280 multi-element neutron-nuclei interactions that produce gamma rays at the same
281 energy that are indistinguishable even when using high energy resolution
282 gamma-ray spectrometers (e.g. HPGe semi-conductor detectors). Unfortunately,
283 it is difficult to deal with these gamma-ray line identification problems when
284 analyzing gamma-ray remote sensing data, because remote sensing gamma-ray
285 spectroscopy is limited by the collection of PHA energy spectra and the use of
286 the constant neutron source resulting from GCR interactions with the planet.

287 However, these gamma-ray line identification problems can be easily addressed
288 with the PING instrument by taking advantage of the pulsed nature of the *in situ*
289 neutron source synchronized with the data acquisition system.

290 Figure 6 shows an example of interfering lines common in gamma-ray PHA
291 energy spectra collected by low energy resolution detectors. Here we see two
292 interfering lines in a gamma-ray spectrum taken using the PING instrument with
293 a LaBr₃ scintillation detector on top of a granite and polyethylene configuration.

294 <Insert Figure 6>

295 The counts in the unresolved peak area are primarily from ²⁸Si and ⁵⁶Fe gamma
296 rays. The natural solution would be to use a gamma-ray spectrometer with better
297 energy resolution, but one does not always have that option due to mass, power,
298 volume and cost constraints associated with planetary space flight missions. One
299 way to remedy this problem is to separate the gamma-ray energy spectra by
300 nuclear process using the gamma-ray event times as shown in Figure 7.

301 <Insert Figure 7>

302 Figure 7 is a plot of four different gamma-ray PHA spectra, with the lines from
303 Table 1 indicated, for a 6.33-hr live time acquisition with the PING instrument
304 using a HPGe detector on the basalt monument, consisting of: 1) a total gamma-
305 ray spectrum (in black) including all neutron-nuclei gamma-ray processes; 2) an
306 inelastic gamma-ray spectrum (in red) created by only selecting gamma-ray
307 events during the PNG pulse for t=20-100 μs; 3) a neutron capture gamma-ray
308 spectrum (in green) created by only selecting gamma-ray events after the PNG
309 pulse for t=150-650 μs; and 4) a delayed activation and natural activity gamma-

310 ray spectrum (in purple) created by only selecting gamma ray events for t=650-
311 999 μ s. Separating the gamma-ray acquisition into different time slices allows us
312 to isolate gamma-ray events for specific interactions from a single element
313 without accumulating excessive background when the peaks are not actually
314 present.

315 <Insert Table 1>

316 Even if a better energy resolution detector like HPGe is used, gamma-ray line
317 identification can still be challenging, due to multi-element neutron-nuclei
318 interactions that produce gamma rays at the same energy but from different
319 elements. For example, Table 2 lists a selected set of gamma-ray line energies
320 and their possible sources from neutron-nuclei interactions with different
321 elements, demonstrating how multiple elements can contribute to the same line
322 energy.

323 <Insert Table 2>

324 Problems with interfering lines can be dealt with by examining the time profile
325 of the individual gamma ray lines. Figure 8a is an example of a 6.33-hr summed
326 HPGe gamma ray spectrum taken with PING instrument on top of the basalt
327 monument. In this spectrum, the Doppler broadened $^{27}\text{Al}(n,n'\gamma)$ gamma ray line
328 from neutron inelastic scattering, the $^1\text{H}(n,\gamma)$ gamma ray line from neutron
329 capture, and the $^{24}\text{Na}(n,\beta\gamma)$ SE from delayed activation are clearly interfering with
330 one another. One way to distinguish $^{27}\text{Al}(n,n'\gamma)$ and the $^1\text{H}(n,\gamma)$ gamma ray lines
331 is by plotting the net peak area of the unresolved spectral feature in Figure 8a as
332 a function of time, as shown in Figure 8b, to distinguish which line is present.

333 Figure 8b shows the time histograms of the net peak areas for the 2211 keV
334 $^{27}\text{Al}(n,n'\gamma)$ and the 2223 keV $^1\text{H}(n,\gamma)$ gamma ray lines. The time histograms are
335 the gamma-ray count rates per 10 μs time interval and demonstrate that one can
336 distinguish between and separate interfering lines by nuclear process to improve
337 both the peak identification and the measurement precision.

338 < Insert Figures 8a and 8b >

339 *3.3 Improved Gamma-Ray Measurement Precision*

340 Separating a gamma-ray spectrum by nuclear process improves the overall
341 gamma-ray line measurement precision. As seen in Table 1 in Section 3.2 many
342 of the time-gated inelastic scattering and capture lines show improved precision
343 as compared with the same lines in the summed spectrum. The 3539 and 4934
344 keV $^{28}\text{Si}(n,\gamma)$ capture lines show improved precision resulting from time-gated
345 analysis. The precision of these Si lines in the summed spectrum, representing
346 results without time slicing, is 8.3% and 16.92%. These same Si lines show
347 improved precision (7.3% and 9.21%) in the capture-delayed activation spectrum
348 obtained with optimized time gating from the removal of the gamma-ray
349 background due to inelastic scattering. A similar but somewhat smaller
350 improvement is seen for the 2211 keV $^{27}\text{Al}(n,n'\gamma)$ inelastic line.

351 An interesting situation is observed for the 1779 keV $^{28}\text{Si}(n,n'\gamma)$ and 6129 keV
352 $^{16}\text{O}(n,n'\gamma)$ inelastic lines shown in Table 1. These gamma rays are also produced
353 in the other two spectra by delayed activation reactions (see Table 2). Therefore,
354 the 1779 and 6129 keV gamma ray lines in the summed spectrum have a better
355 statistical precision of 0.48% and 1.10% as compared to 1.00% and 1.67%

356 (inelastic spectrum) and 0.52% and 1.42% (capture-delayed activation spectrum),
357 because there are more counts in the summed spectrum.

358 The 1779 and 6129 keV lines are not as useful for determining elemental
359 weight percent, because they have a large contribution due to delayed activation.
360 However, the data in the capture-delayed activation spectrum can be used to
361 correct the data in the inelastic spectrum for the portion of the counts that are
362 due to inelastic scattering. While this correction leads to a deterioration of the
363 statistical precision of the weight percent determination from the inelastic data, it
364 provides elemental concentrations that have dramatically improved accuracy.

365 *3.4 Identifying and Removing Sources of Systematic Error Using TLIST data*

366 Space-based planetary science missions are unique, because there is usually
367 only one opportunity to collect data. Gamma ray and neutron spectroscopy
368 remote sensing measurements are further restricted to only gamma rays or
369 neutrons produced by a constant neutron flux source created by GCR
370 interactions with the planetary surface and atmosphere. With a weak constant
371 neutron source there is no need to record event-by-event time and energy data if
372 the data are transferred periodically with reasonable frequency, since each chunk
373 of transferred data can be separately analyzed to identify a problem with the
374 instrument, e.g. deteriorated resolution, and removed without compromising the
375 entire concatenated data set. However, it is still difficult to determine if the
376 collected data have been compromised due to other errors. These difficulties
377 can be mitigated for the case of *in situ* gamma-ray and neutron spectroscopy
378 measurements with the PING instrument, since it takes advantage of a pulsed

379 neutron generator synchronized with gamma ray and neutron detector data
380 acquisition combined with the ability to post-process acquired time-tagged event-
381 by-event data.

382 A unique benefit of incorporating a pulsed neutron generator with a time-tagged
383 event-by-event data acquisition system is that regions in time containing
384 suspicious data can be isolated and removed from the data set for further
385 inspection without affecting the usefulness of the remaining data. Systematic
386 errors in data are nearly impossible to anticipate but often can be identified when
387 examining the post-processed data. Examples include systematic errors caused
388 by equipment operating parameter changes, such as temperature effects on a
389 detector response or, as illustrated in the data shown in Table 3 below, changes
390 in the time-dependence of the turn on of neutron-induced gamma-ray flux that
391 occurs during the PNG burst period.

392 < Insert Table 3 >

393 We demonstrate the merit of saving event-by-event time and energy data with
394 our analysis of the gamma-ray count rate of the 6129 keV peak from neutron
395 inelastic scattering on ^{16}O for a 2-hr live time gamma-ray acquisition by the PING
396 instrument set-up on the basalt monument. Since the neutron inelastic scattering
397 gamma-ray production rate is proportional to the fast neutron flux, we assume
398 that a stable gamma-ray count rate can be obtained from the time the “pulse start”
399 signal is given to the PNG ion source ($t = 0 \mu\text{sec}$). We can examine the time
400 dependence of the fast neutron-induced gamma-ray flux from the time of the

401 “pulse start” signal to the end of the PNG pulse ($t = 0$ to $100 \mu\text{sec}$) to look for
402 anomalies.

403 In this example, we generated gamma-ray energy spectra for each of ten time
404 slices (time slice width = $10 \mu\text{sec}$) of the gamma-ray data during the PNG pulse
405 and determined the 6129 keV net gamma-ray peak count rate and its associated
406 uncertainty for each time slice. Table 3 lists the time range for each time slice,
407 the 6129 keV peak count rates and the uncertainty in the count rates for each of
408 the ten time slices. Note that the count rates in the first and second time slices
409 are inconsistent with the count rates in the 8 other time slices and that the count
410 rate for these later 8 time slices is constant as expected.

411 The low 6129 keV gamma-ray count rate during the first time slice ($t = 0$ - 10
412 microseconds) indicates that the PNG has not begun producing fast neutrons yet,
413 since there is a delay between the time that the PNG is sent the “burst on”
414 command signal and the time when fast neutrons are actually being generated
415 by the PNG. The higher 6129 keV gamma-ray count rate in the second time
416 slice ($t = 10$ - 20 microseconds) is also inconsistent with the average value for the
417 other slices and may be due to a systematic error induced by the gamma-ray
418 detector electronics. In both cases, we can choose to exclude these data points
419 from further analysis, since they are not representative of the constant inelastic
420 gamma-ray flux during the PNG pulse.

421 To be sure, we would investigate the origin of the systematic errors that
422 prompt us to remove the data from the main analysis. Without this event-by-
423 event time and energy data, however, these points would have been unexamined

424 and included in the data, skewing the results. Excluding the data from the first 20
425 μs will increase the statistical error on the mean value of the 6129 keV gamma-
426 ray production rate, but will result in more accurate data that we can use to infer
427 the bulk elemental composition of planetary material. This is clearly seen by
428 comparing the 6129 keV weighted mean count rate and uncertainty for time
429 slices 3 through 10 ($t = 20 - 100 \mu\text{s}$) which is $42.2 \text{ cts}/\mu\text{s} \pm 1.10 \text{ cts}/\mu\text{s}$ versus the
430 6129 keV weighted mean count rate and uncertainty for time slices 1 through 10
431 ($t = 0 - 100 \mu\text{s}$) which is $30.1 \text{ cts}/\mu\text{s} \pm 0.82 \text{ cts}/\mu\text{s}$. The difference between these
432 two averages is almost ten times the statistical uncertainty, resulting in a very
433 significant systematic error that would compromise the accuracy of derived
434 elemental concentrations.

435

436 **4. Conclusions**

437 Many of the problems typically encountered by planetary gamma-ray
438 elemental composition measurements are addressed by using PING in event-by-
439 event data acquisition mode. For example, it is generally impossible to know *a*
440 *priori* how to set optimum time windows for gamma-ray detection when using a
441 pulsed neutron generator as the source of neutrons, because of compositional
442 variations from location to location on a planetary body. This is a real problem
443 because there is usually only one opportunity to acquire a specific set of data
444 during planetary missions. This problem is solved when taking data in an event-
445 by-event mode, because data can be analyzed after it is collected and therefore
446 set optimum time windows based on the data.

447 Our goal is to obtain the best estimate of elemental concentrations from the
448 gamma-ray data. However, the same energy gamma ray can often be created
449 from different isotopes via two different reaction mechanisms. In such instances
450 we can separate out different time regions where a particular gamma ray is due
451 to a specific reaction mechanism.

452 Post-processing event-by-event data allows PING to obtain the best precision
453 and most accurate results. For example, in the analysis of a peak that only
454 occurs in one time region, one can reduce its uncertainty by ~40% by eliminating
455 background in that energy region that occurs at times when the peak is not
456 present. Perhaps even more important is the improvement in accuracy that can
457 be achieved when the same gamma ray peak can be obtained at different times
458 from different reaction mechanisms. The inelastic window in Table 1 for the 1779
459 gamma-ray peak is largely from the $^{28}\text{Si}(n,n'\gamma)$ reaction. However this area must
460 be corrected for the delayed activity present. The result is a factor of 3 smaller
461 than the 1779 keV area for the entire time spectrum, but the reduced area can
462 now be converted to weight percent Si.

463 Another improvement in the accuracy of the results can be obtained by
464 eliminating data when it appears the instrument is not performing properly as
465 shown in Table 3 and discussed in Section 3.4. For example, the 6129 keV
466 weighted mean average for 0-100 μs is $30.1 \text{ cts}/\mu\text{s} \pm 0.82 \text{ cts}/\mu\text{s}$ and for 20-100
467 μs is $42.2 \text{ cts}/\mu\text{s} \pm 1.10 \text{ cts}/\mu\text{s}$. Although the statistical error of the weighted
468 mean average increases when you exclude the first 20 μs , the difference
469 between these two averages is almost ten times the statistical uncertainty and

470 would significantly impact the accuracy of the derived bulk elemental
471 concentrations of planetary material.

472 We can also minimize instrumental problems by subdividing the total data set
473 at certain times to investigate such things as gain shifts. Thus by independently
474 analyzing subsets of the data, you can preserve data quality that would be
475 compromised if you were limited to only analyzing PHA data.

476 When using a pulsed neutron source, the potential exists for obtaining higher
477 precision data. By using event-by-event data acquisition, the risk of improper
478 timing settings is eliminated and systematic errors can be reduced or eliminated.
479 Taken together, event-by-event data acquisition of pulsed neutron-induced
480 gamma ray spectra for determining elemental concentrations, provides significant
481 enhancements to measurements obtained on a planetary surface resulting in the
482 best scientific information on a particular mission.

483

484 **Acknowledgements**

485 We would like to thank S.L. Floyd, M. Namkung, and S.F. Nowicki for assistance
486 with acquiring the data. We would like to thank R. Forsythe for assistance with
487 the data analysis. We would like to thank J.I. Trombka and T.P. McClanahan for
488 many useful discussions. We are indebted to NASA, NSF, and the Tennessee
489 Space Grant for partial support of this research.

490

491

492

493 **References**

- 494 [1] W.C. Feldman, et al., J. Geophys. Res. 109 (2004) E07S06.
- 495 [2] W.V. Boynton, et al., Space Sci. Rev. 110 (2004) 37.
- 496 [3] W.V. Boynton, et al., Science 297 (2002) 81.
- 497 [4] T.H. Prettyman, et al., IEEE Trans. Nucl. Sci. N50 (2003) 1190.
- 498 [5] J.O. Goldsten, et al., Space Sci. Rev. 131 (2007) 339.
- 499 [6] L.G. Evans, et al., MAPS 36 (2001) 1639.
- 500 [7] I.G. Mitrofanov, et al., Space Sci. Rev. 150 (2010) 183.
- 501 [8] I.G. Mitrofanov, et al., Astrobiology 8 (2008) 793.
- 502 [9] A. Parsons, et al., Nucl. Instr. and Meth. A 652 (2011) 674.
- 503 [10] A.E. Metzger, et al., Science 179 (1973) 800.
- 504 [11] L. Szentmiklosi, et al., J. Radioanal. Nucl. Chem. 262 (2005) 213.
- 505 [12] J.A. Grau, et al., IRRMA '92, Raleigh, NC, 8-11 Sept., 1992; Int. J. Rad. Appl.
- 506 Instr. Part E, 7 (1993) 173.
- 507 [13] D.B. Pelowitz, et al., (2005) MNCPX User's Manual, Version 2.5.0, LANL,
- 508 Los Alamos, LA- UR-05-0369.
- 509 [14] J. Bodnarik, et al., 41st LPSC, Woodlands, TX, 1-5 Mar., 2010; Conf. Proc.
- 510 41 (2010) 2581.
- 511 [15] P. Ann, et al., 2011 IEEE (NSS/MIC), Valencia, Spain, 23-29 Oct., 2011;
- 512 IEEE Conf. Rec. (2011) 1234, doi: 10.1109/NSSMIC.2011.6154608.
- 513 [16] CANBERRA Lynx Digital Signal Analyzer application note (2012)
- 514 <http://www.canberra.com/literature/438222.asp>.

- 515 [17] J.G. Bodnarik, et al., 2010 IEEE (NSS/MIC), Knoxville, TN, 30 Oct. – 6 Nov.,
516 2010; IEEE Conf. Rec. (2010) 1, doi: 10.1109/NSSMIC.2010.6036247.
- 517 [18] D. Burger, personal communication, 2011.
- 518 [19] D.L. Chichester, et al., J. Radioanal. Nucl. Chem. 271 (2007) 629.
- 519

520 **Figure Captions and Titles**

521

522 **Figure 1. Illustration of PING.** The instrument is mounted on the underside of a
523 planetary surface rover. Also shown are the different nuclear processes that
524 produce the gamma rays and scattered neutrons that are detected at the surface.

525

526 **Figure 2. Aerial view of GGAO.** This schematic of the outdoor gamma ray and
527 neutron instrumentation testing facility shows the operations control building as
528 well as the 46 m diameter safety perimeter surrounding the two existing 1.8 m x
529 1.8 m x 0.9 m granite and basalt monuments.

530

531 **Figures 3. Timing Windows and Sample Spectra.** a) Placement of timing
532 windows relative to each PNG pulse. b) Examples of different spectral shapes
533 seen in different timing windows.

534

535 **Figure 4. Images of MultiScan Screens.** MultiScan was written using the Java
536 programming language, the NetBeans integrated development environment
537 (IDE), and the Lynx software development kit (SDK).

538

539 **Figure 5. PING Experiment Set-up.** PING deployed for measurements on top
540 of the basalt monument. The PNG is on the left, the HPGe detector is on the
541 right, and ^3He detectors are between them. The data acquisition electronics are
542 situated behind the basalt and are not visible in this photo.

543 **Figure 6. LaBr₃ Spectrum.** An example of unresolved lines in a portion of a
544 gamma ray spectrum taken using the PING instrument with a LaBr₃ scintillation
545 detector on top of a granite and polyethylene configuration.

546

547 **Figure 7. Spectra from Different Time Windows.** Gamma-ray spectra from a
548 6.33-hr acquisition using a HPGe detector on top of Columbia River basalt.

549

550 **Figure 8. Spectral Feature and Time Distribution.** a) A portion of the non-time
551 sliced 6.33-hr gamma ray energy histogram from PING data taken on the bare
552 basalt monument. b) Time histogram showing how one can get better precision
553 on the net peak area of each line, shown in Table 1, by analyzing their respective
554 energy histograms during different time slices during the PNG pulse period.

555

556

557

558

559

560

561

562

563

564

565 **Table Captions**

566

567 Table 1. HPGe gamma-ray line intensities (I_g) and uncertainties (s) for a 6.33-hr

568 PING acquisition on the bare Columbia River basalt monument.

569

570 Table 2: γ -ray lines to analyze for inelastic γ -ray spectra time window

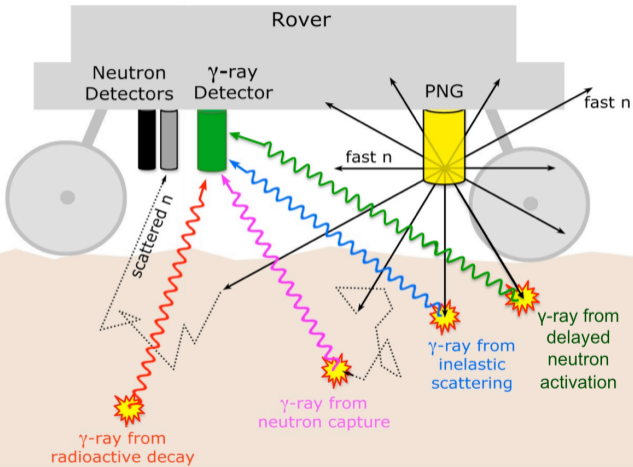
571 optimization.

572

573 Table 3. Fast neutron induced count rate and uncertainty for the 6129 keV

574 $^{16}\text{O}(n,n'\gamma)$ gamma ray peak for ten time slices during the PNG pulse.

Figure(s) 1



Figure(s) 2

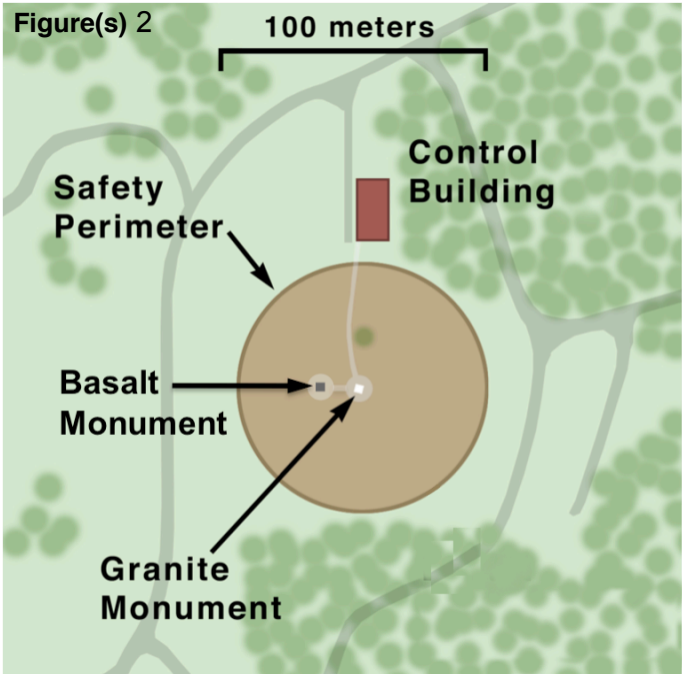
100 meters

**Safety
Perimeter**

**Control
Building**

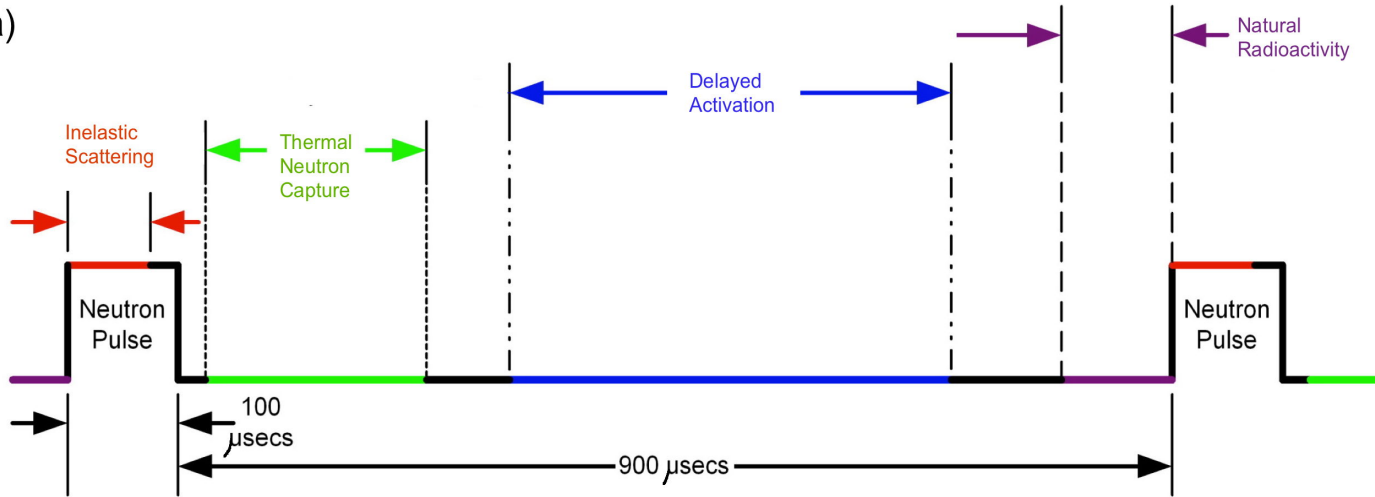
**Basalt
Monument**

**Granite
Monument**

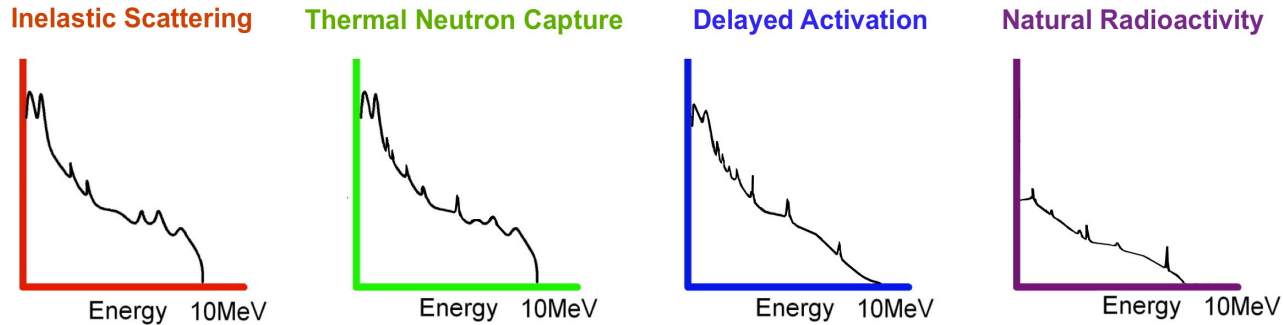


Figure(s) 3

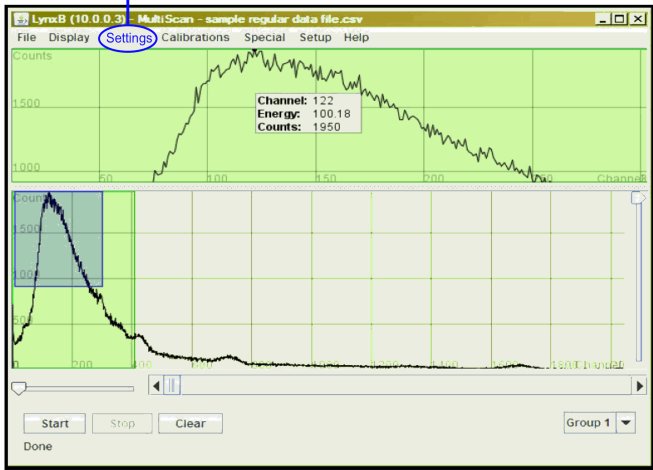
a)



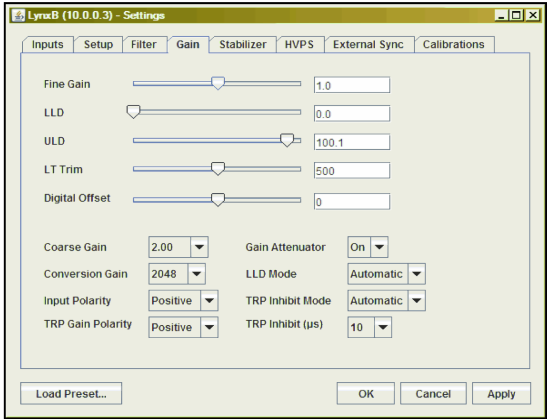
b)



Figure(s) Analyzing a test spectrum: Zooming in on a specific area & highlighting a peak

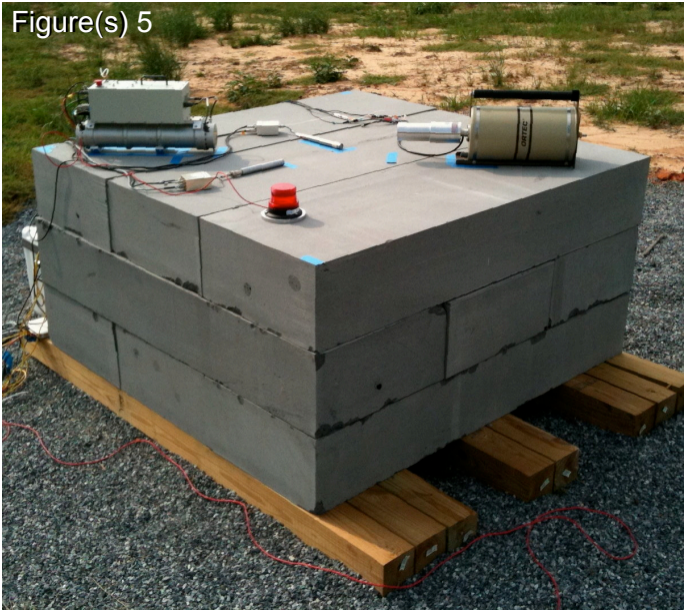


Checking settings: View & modify settings quickly & easily.

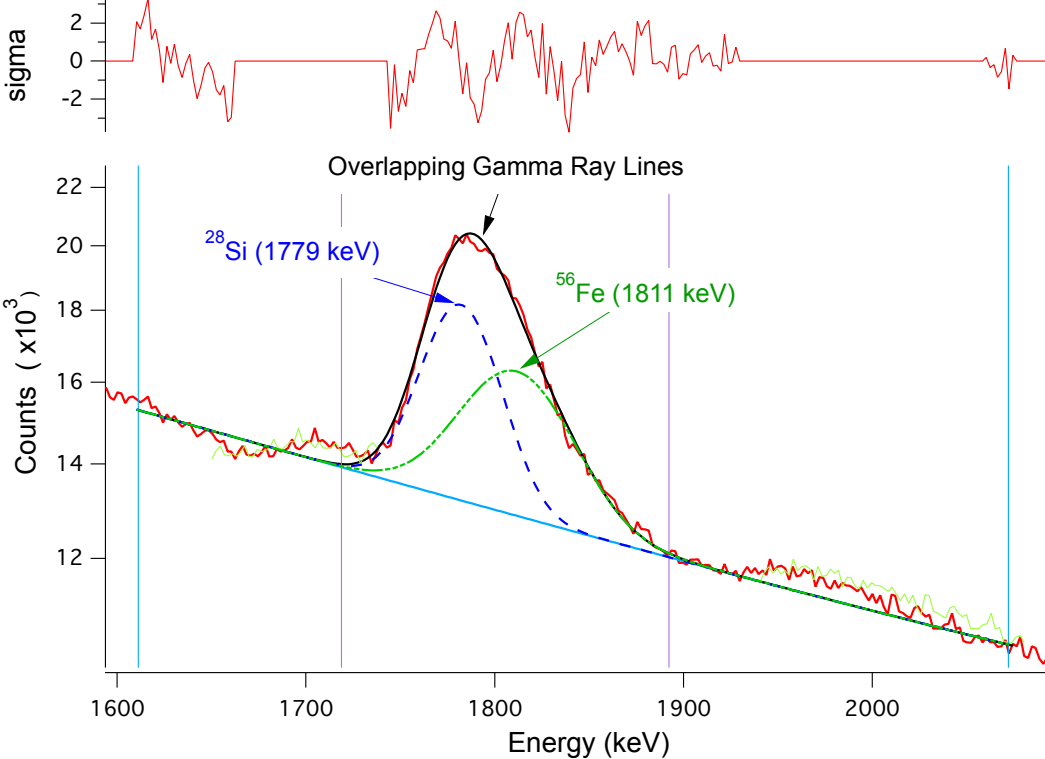


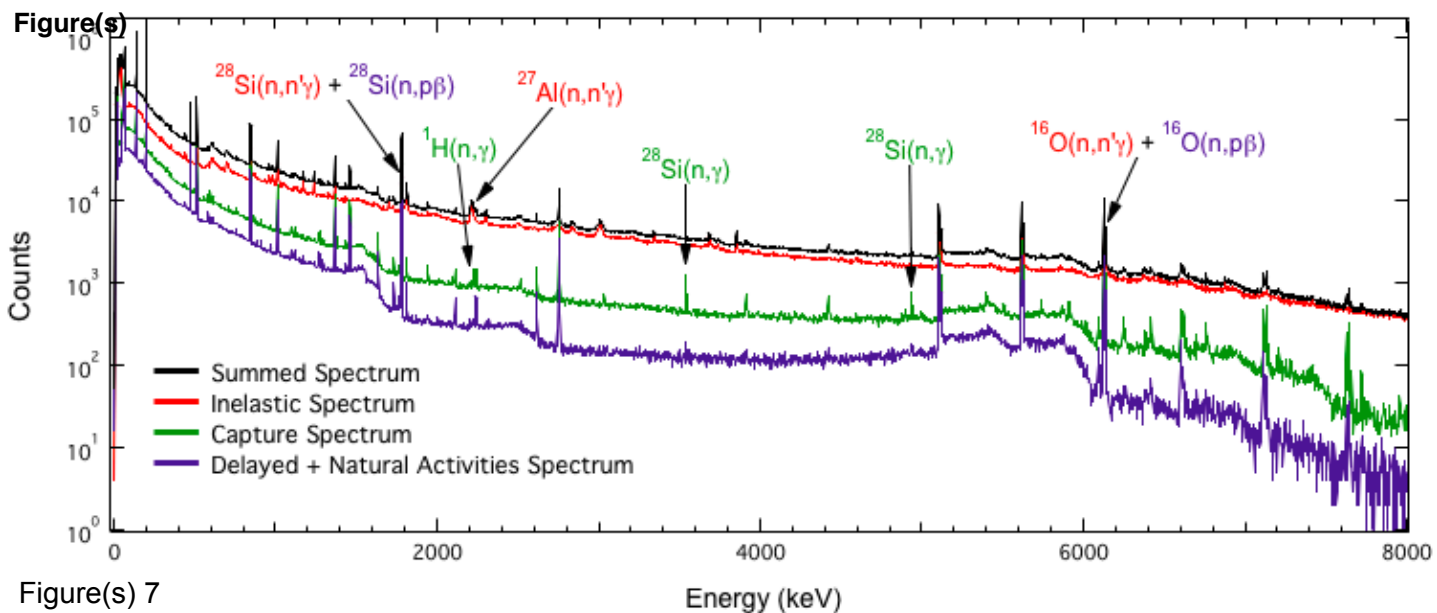
Figure(s) 4

Figure(s) 5



Figure(s) 6





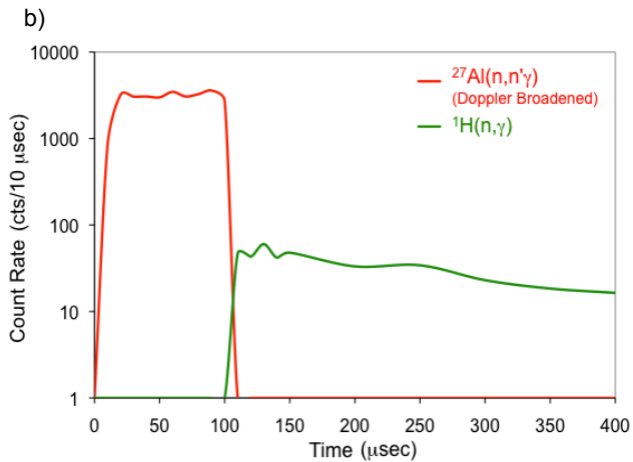
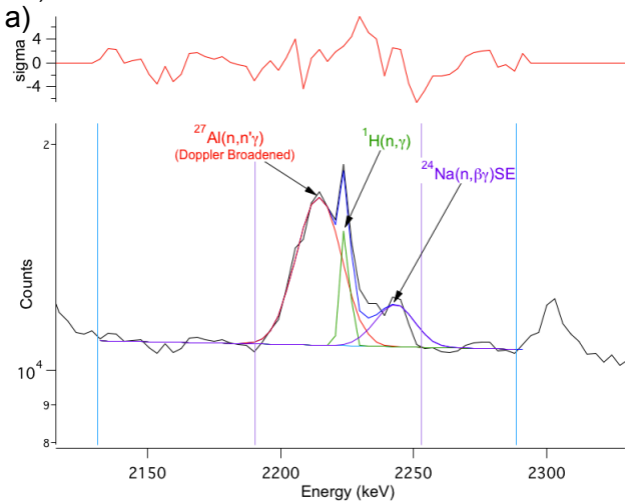
Figure(s) 8

Table 1. HPGe gamma-ray line intensities (I_γ) and uncertainties (σ) for a 6.33-hr PING acquisition on the bare Columbia River basalt monument.

| Energy (keV) | Summed | | Inelastic Scattering | | | Capture – Activation | | |
|-----------------|------------------|--------------|------------------------------|------------------|--------------|---|------------------|--------------|
| | I_γ (cts) | σ (%) | ID | I_γ (cts) | σ (%) | ID | I_γ (cts) | σ (%) |
| 1779 | 90480 | 0.48 | $^{28}\text{Si}(n,n'\gamma)$ | 31730 | 1.00 | $^{28}\text{Si}(n,p\beta)$ $^{27}\text{Al}(n,\gamma\beta)$ | 57980 | 0.52 |
| 2211 | 24310 | 1.55 | $^{27}\text{Al}(n,n'\gamma)$ | 23760 | 1.50 | | | |
| 2223 | 1892 | 16.10 | $^1\text{H}(n,\gamma)$ | 967 | 14.50 | $^1\text{H}(n,\gamma)$ | 887 | 7.40 |
| 3539 | 1154 | 8.30 | | | | $^{28}\text{Si}(n,\gamma)$ | 1158 | 7.30 |
| 4934 | 1472 | 16.90 | | | | $^{28}\text{Si}(n,\gamma)$ | 1151 | 9.21 |
| 6129 | 19920 | 1.10 | $^{16}\text{O}(n,n'\gamma)$ | 10900 | 1.67 | $^{16}\text{O}(n,p\beta)$ | 9087 | 1.42 |

Table 2: γ -ray lines to analyze for inelastic γ -ray spectra time window optimization

| Gamma-Ray Lines (keV) | Possible Sources of Neutron Nuclei Interactions |
|-----------------------|---|
| 843 | A, B, C, D, E |
| 1014 | A, D |
| 1779 | F, G, H |
| 1811 | B, C, E |
| 2211 | A |
| 6129 | I, J |

Key:

A: $^{27}\text{Al} (n, n'\gamma) ^{27}\text{Al}$
B: $^{56}\text{Fe} (n, n'\gamma) ^{56}\text{Fe}$
C: $^{56}\text{Fe} (n, p) ^{56}\text{Mn} (\beta) ^{56}\text{Fe}$
D: $^{26}\text{Mg} (n, \gamma) ^{27}\text{Mg} (\beta) ^{27}\text{Al}$
E: $^{55}\text{Mn} (n, \gamma) ^{56}\text{Mn} (\beta) ^{56}\text{Fe}$
F: $^{28}\text{Si} (n, n'\gamma) ^{28}\text{Si}$
G: $^{28}\text{Si} (n, p) ^{28}\text{Al} (\beta) ^{28}\text{Si}$
H: $^{27}\text{Al} (n, \gamma) ^{28}\text{Al} (\beta) ^{28}\text{Si}$
I: $^{16}\text{O} (n, n'\gamma) ^{16}\text{O}$
J: $^{16}\text{O} (n, p) ^{16}\text{N} (\beta) ^{16}\text{O}$

Table 3. Fast neutron induced count rate and uncertainty for the 6129 keV $^{16}\text{O}(n,n'\gamma)$ gamma ray peak for ten time slices during the PNG pulse.

| Time Slice | Time Range (μs) | Count Rate (cts/μs) | Uncertainty (cts/μs) |
|-------------------|--|--|---|
| 1 | 0 - 10 | 9 | ± 1 |
| 2 | 10 - 20 | 55 | ± 4 |
| 3 | 20 - 30 | 41 | ± 3 |
| 4 | 30 - 40 | 42 | ± 3 |
| 5 | 40 - 50 | 39 | ± 3 |
| 6 | 50 - 60 | 42 | ± 3 |
| 7 | 60 - 70 | 41 | ± 3 |
| 8 | 70 - 80 | 41 | ± 3 |
| 9 | 80 - 90 | 46 | ± 3 |
| 10 | 90 - 100 | 45 | ± 3 |